

# Ages and Metallicities of Hickson Compact Group Galaxies

Robert. N. Proctor<sup>1</sup>, Duncan. A. Forbes<sup>1</sup>, George. K. T. Hau<sup>2</sup>, Michael. A. Beasley<sup>1</sup>,  
G. M. De Silva<sup>1</sup>, R. Contreras<sup>3</sup> and A. I. Terlevich<sup>4</sup>

<sup>1</sup> Centre for Astrophysics & Supercomputing, Swinburne University, Hawthorn VIC 3122, Australia

Email: rproctor@astro.swin.edu.au, dforbes@swin.edu.au

<sup>2</sup> European Southern Observatory, Garching, Germany

<sup>3</sup> Departamento de Astronomia y Astrofisica, P. Universidad Catolica, Casilla 104, Santiago 22, Chile

<sup>4</sup> School of Physics and Astronomy, University of Birmingham, Birmingham, B15 2TT, UK

17 January 2022

## ABSTRACT

Hickson Compact Groups (HCGs) constitute an interesting extreme in the range of environments in which galaxies are located, as the space density of galaxies in these small groups are otherwise only found in the centres of much larger clusters. The work presented here uses Lick indices to make a comparison of ages and chemical compositions of galaxies in HCGs with those in other environments (clusters, loose groups and the field). The metallicity and relative abundance of ‘ $\alpha$ -elements’ show strong correlations with galaxy age and central velocity dispersion, with similar trends found in all environments. However, we show that the previously reported correlation between  $\alpha$ -element abundance ratios and velocity dispersion disappears when a full account is taken of the the abundance ratio pattern in the calibration stars. This correlation is thus found to be an artifact of incomplete calibration to the Lick system.

Variations are seen in the ranges and average values of age, metallicity and  $\alpha$ -element abundance ratios for galaxies in different environments. Age distributions support the hierarchical formation prediction that field galaxies are on average younger than their cluster counterparts. However, the ages of HCG galaxies are shown to be more similar to those of cluster galaxies than those in the field, contrary to the expectations of current hierarchical models. A trend for lower velocity dispersion galaxies to be younger was also seen. This is again inconsistent with hierarchical collapse models, but is qualitatively consistent with the latest N-body-SPH models based on monolithic collapse in which star formation continues for many Gyr in low mass halos.

**Key words:** galaxies: interactions - galaxies: elliptical - galaxies: evolution

## 1 INTRODUCTION

Hickson Compact Groups (HCGs) were defined by Hickson (1982) to be spatially compact collections of four or more galaxies that are relatively isolated from their general surroundings. The original selection was made without knowing individual redshifts of the galaxies. Consequently a few galaxies have been shown to be merely chance projections. Although claims were made that such projections were a major contributor to the appearance of HCGs (e.g. Mamon 1986; Hernquist, Katz & Weinberg 1995), the reality of most HCGs is now accepted (e.g. Ponman *et al.* 1996; Tovmassian *et al.* 2000).

The space density of galaxies in HCGs is very high, and comparable to that at the centres of galaxy clusters. Furthermore the velocity dispersions within HCGs are quite low ( $\sim 200$  km s<sup>-1</sup>). These two conditions imply that HCGs

are the galactic environments in which the effects of mergers and interactions should be most pronounced. Signs of mergers and interactions have indeed been found in HCGs (e.g. Rubin, Hunter & Ford 1991; Forbes 1992; Mendes de Oliveira & Hickson 1994; Jones, Ponman & Forbes 2000). However, the merging rates and starburst/AGN activity seem to be lower than expected (Zepf & Whitmore 1991; Coziol *et al.* 1997; Verdes-Montenegro *et al.* 1998). It has also been shown (Ponman *et al.* 1996) that most HCGs are nearly or fully virialized systems, indicating that most are fairly evolved. This is surprising, given the short crossing times in most HCGs, as such groups should be unstable and merge into a single massive galaxy within the Hubble time (White 1990). These considerations have prompted speculation about the formation and evolution of HCGs. One possibility is that the galaxies do merge, and form a single massive ellipti-

cal galaxy, but, with secondary infall of surrounding galaxies, the systems maintain their status as HCGs (Governato, Tozzi & Cavaliere 1996). A second possibility is that loose groups may be continuously collapsing to form more compact groups (Diaferio, Gell & Ramella 1994). Alternatively, simulations suggest that if the dark matter is distributed in a common group halo, rather than individual galaxy halos, merging is suppressed and HCGs would be dynamically long-lived systems (Athanasoula, Makino & Bosma 1997).

It is also useful to consider the predictions of the various models of galaxy formation. For instance, Kauffmann (1996) used a semi-analytical approach to modeling the hierarchical formation of galaxies in different environments, finding a bimodal age distribution in dark matter halos of size  $10^{13} M_{\odot}$ , which includes HCGs, small group and field galaxies. In such halos the Kauffmann models predict the central luminous ellipticals to have younger average ages than their less luminous neighbours. On the other hand, the N-body-SPH monolithic collapse models of elliptical galaxy formation of Chiosi & Carraro (2002) predict younger ages for low mass galaxies than for those with high mass.

One way to discriminate between the different evolutionary models would be to determine ages and chemical compositions of a number of early-type galaxies in HCGs for comparison to those of galaxies in other environments. For example, are they generally old (indicating a low interaction rate) like galaxies in the centre of clusters, or is there evidence of an enhanced interaction rate as indicated by the younger stellar populations often seen in loose group and field galaxies?

In this paper we use an approach which has been successfully applied to galaxies in clusters, loose groups and the field, i.e. using Lick indices to obtain relative ages and metallicities (e.g. Gonzalez 1993; Kuntschner 2000; Trager *et al.* 2000, hereafter T00; Poggianti *et al.* 2001; Kuntschner *et al.* 2002; Proctor & Sansom 2002, hereafter PS02; Terlevich & Forbes 2002). Here we extend these techniques to HCGs for the first time. The results for HCGs are compared to galaxies in different environments and the predictions of galaxy formation models. We assume  $H_0=75 \text{ km s}^{-1} \text{ Mpc}^{-1}$  throughout.

## 2 THE SAMPLE

Groups were chosen from the Hickson Compact Group Catalog (Hickson 1982). The groups were HCG 4, 14, 16, 22, 25, 32, 40, 42, 62 and 86. The spectra of several galaxies not in HCGs were also obtained. These include three field Arp-Madore galaxies NGC 2502, NGC 3203 and NGC 6684, 2 galaxies in the massive loose group NGC 5044, and NGC 3305 located in the loose group LGG211 (Garcia 1993). Our emphasis was to obtain spectra for the early-type galaxies. However, a number of spiral galaxies were also observed. A number of galaxies failed to achieve a suitable signal-to-noise and have been omitted (see Section 4). The remaining galaxies exhibit signal-to-noise ratios of between 20 and 60. These include a total of 17 early-type galaxies and 9 spiral bulges in HCGs, and 6 early-type galaxies in groups.

Galaxy	Date	Exp. time (secs)	P.A. (degrees)
<b>2000 Apr Long-slit</b>			
HCG62:ZM19	2000/04/09	3x600	117
NGC 5046	2000/04/11	2x600	50
NGC 5049	2000/04/11	4x600	33
NGC 6684	2000/04/09	3x600	125
<b>2000 Apr MOS</b>			
HCG42A	2000/04/09	3x1200	108
HCG42C	2000/04/09	3x1200	108
HCG86A	2000/04/11	3x1200	118
HCG86B	2000/04/11	3x1200	118
<b>2001 Jan Long-slit</b>			
HCG62:ZM22	2000/12/30	3x600	80
HCG40B	2000/12/31	3x600	10
NGC 2502	2001/01/01	3x600	30
NGC 3203	2001/01/01	2x600	330
NGC 3305	2001/01/01	3x600	270
<b>2001 Jan MOS</b>			
HCG4A	2000/12/30	3x1200	0
HCG4C	2000/12/30	3x1200	0
HCG14A	2001/01/01	3x1200	0
HCG14B	2001/01/01	3x1200	0
HCG16A	2000/12/31	3x1200	90
HCG16B	2000/12/31	3x1200	90
HCG16X	2000/12/31	3x1200	90
HCG22A	2000/12/30	3x1200	30
HCG22B	2001/01/01	3x1200	330
HCG22D	2000/12/30	3x1200	30
HCG22E	2000/12/30	3x1200	30
HCG22X	2001/01/01	3x1200	330
HCG25B	2000/12/31	3x1200	0
HCG25F	2000/12/31	3x1200	0
HCG32A	2000/12/30	3x1200	330
HCG32B	2000/12/30	3x1200	330
HCG32D	2000/12/30	3x1200	330
HCG40A	2000/12/31	3x1200	0
HCG40D	2000/12/31	3x1200	0

**Table 1.** Observational parameters for both the 2000 and 2001 observing runs. HCG16X is a previously unidentified galaxy projected close to HCG16D at  $\alpha=02^h 09^m 46.6^s$ ,  $\delta=-10^\circ 11' 00.7''$  (J2000). Its membership of HCG16 is confirmed by its recession velocity (see Table 2). HCG22X has a 2MASS identification of J03032308-1539079. The ZM identification refers to Zabludoff & Mulchaey (1998).

## 3 OBSERVATIONS AND INITIAL DATA REDUCTION

Spectra were obtained on the ESO NTT telescope on 2000 April 9-11th and 2000 Dec. 30-31st – 2001 Jan. 1st (hereafter 2001 Jan run). Table 1 summarises the observational parameters. Seeing was around 1 arcsec for both observing runs. The observations consist of a combination of long-slit and multi-object spectrograph (MOS) spectra obtained using the red arm of the EMMI instrument. All MOS masks had a slit-width 1.87 arcsec. Long-slit spectra (slit-width 2.0 arcsec) were taken of additional galaxies not covered by the MOS observations. In general, slits were not aligned along a preferred axis of the galaxies. All spectra were taken with ESO Grism# 5 and cover the wavelength range from  $\sim 4000$

to 6600 Å. This wavelength range covers 25 Lick indices. However, redshift and vignetting effects cause the loss of indices at the extremes of this range. The spectral resolution was 6.4Å FWHM. Spectra of seven Lick standard stars, as well as spectrophotometric standards, were taken during the runs. Exposures of a He+Ar lamp, with an order sorting filter BG38, were taken for wavelength calibrations. Dome and sky flats were obtained for flat-fielding.

Initial data reductions were carried out using standard tasks within IRAF. Briefly, the data were bias-subtracted, trimmed, bad pixels and cosmic rays removed, and flat-fielding carried out using dome flats. Individual spectra were then extracted and sky-subtracted using the *apall* task. Sky-subtractions in MOS data are notoriously difficult, and despite careful selection of sky regions, sky-line residuals were evident in some MOS spectra after sky-subtraction. The method of analysis of these spectra was therefore designed to detect and ameliorate the effects of such residuals (see Section 5). Spectra were extinction corrected and flux calibrated using flux standard stars observed over several nights. For each galaxy we obtained three spectra of the same exposure time. These were co-added before extraction of the central regions. The extraction aperture was 10 pixels (2.7") wide for both the long-slit and MOS spectra.

Determination of recession velocity and velocity dispersion in galaxies was carried out using the IRAF task *fxcor*. The results of these determinations are given in Table 2. A comparison of velocity dispersion measurements with values published in Hypercat (<http://www-obs.univ-lyon1.fr/hypercat/>) are shown in Fig. 1. In this plot the data given in Table 2 have been aperture corrected to an effective aperture size of 1.19  $h^{-1}$  kpc according to Jørgensen *et al.* (1995). The effective aperture is approximated in Jørgensen *et al.* (1995) by  $D=2.05 \times (xy/\pi)^{1/2}$ . This yields effective apertures of 2.6" for the MOS data and 2.7" for the long-slit data. The average value (2.65") was used for aperture corrections. The estimated extent of these apertures (in kiloparsec) are given in Table 2. Fig. 1 shows that comparisons between aperture corrected values of  $\log \sigma$  from this study and those given in Hypercat are generally within errors.

#### 4 MEASUREMENT OF LICK INDICES

Raw Lick indices were measured using our own code (see PS02). The code measures indices at the wavelength dependent resolution detailed in Worthey & Ottaviani (1997). The measured indices at this point still require correcting for both velocity dispersion and differences in flux calibration between our study and the Lick system.

##### 4.1 Calibration to the Lick system

The procedure used for correcting Lick indices for galaxy velocity dispersion was the same as that given in PS02. Briefly, for galaxies in which the velocity dispersion, when combined in quadrature with the instrumental broadening, resulted in a resolution *higher* than that of the Lick system, the galaxy spectra were convolved with an appropriate Gaussian prior to index measurement. This procedure is clearly not applicable to galaxies in which the combined resolution exceeded that of Lick system. Therefore, indices were measured in

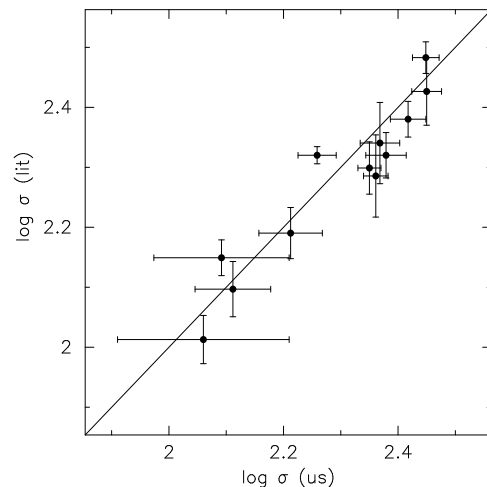


**Figure 1.** Velocity dispersion estimates are compared to values from Hypercat (with the exception of HCG32A, which was taken from de la Rosa, Carvalho & Zepf 2001a). The one-to-one line is also shown. Good agreement with literature values is achieved.

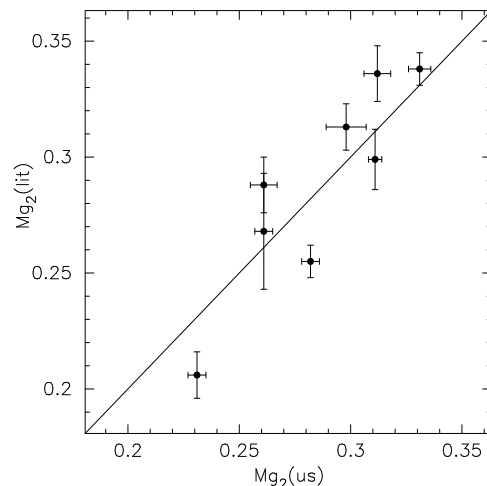


**Figure 2.** Comparison of  $Mg_2$  values from Hypercat with those measured here (aperture corrected). The one-to-one line is also shown. Reasonable agreement with literature values is achieved.

7 Lick standard stars after convolving the spectra with a series of Gaussians of known widths. This permits estimation of correction factors for indices in these galaxies. The method of calculating the correction factors was the same as detailed in PS02. The results from the present study were almost identical to those of PS02, as well as those given in Kuntschner (2000).

The final correction required in order to fully calibrate to the Lick system is to allow for differences in flux calibration. To estimate this correction, Lick indices were measured in each of the observed 7 Lick standard stars. Stars were broadened to the appropriate Lick resolution prior to index measurement (see PS02). The difference between our measurements of the Lick standard stars and those taken on the Lick/IDS system (Worthey *et al.* 1994) are given in Table 3. Differences are generally smaller than the scatter and typical rms error per observation of the Lick calibrators (Worthey *et al.* 1994). Nonetheless, these offsets were

Name	Run	Type	B (mag)	Velocity (km/s)	$M_B$ (mag)	$\sigma$ (km/s)	Aperture (kpc)
<b>Loose Group</b>							
NGC 3305 (LGG211)	2001 Jan LS	E0	13.77	3982	-19.9	242(16)	0.68
NGC 5046	2000 Apr LS	E	13.68	2209	-18.7	135(24)	0.38
NGC 5049	2000 Apr LS	S0	14.75	2958	-18.2	122(18)	0.51
<b>Field</b>							
NGC 2502	2001 Jan LS	SB0	13.26	1093	-17.6	169(36)	0.19
NGC 3203	2001 Jan LS	S0	13.10	2503	-19.4	128(21)	0.43
NGC 6684	2000 Apr LS	SB0	11.31	846	-19.0	119(21)	0.14
<b>Compact Group</b>							
HCG4C	2001 Jan MOS	E	16.08	18306	-20.9	182(19)	3.14
HCG16X	2001 Jan MOS	-	-	3986	-	76(13)	0.68
HCG22A	2001 Jan MOS	E	12.85	2662	-19.9	188(22)	0.46
HCG22D	2001 Jan MOS	SB0	15.28	9268	-20.2	236(16)	1.59
HCG22E	2001 Jan MOS	E	15.85	9579	-19.7	168(19)	1.64
HCG22X	2001 Jan MOS	-	-	9244	-	242(20)	1.58
HCG25F	2001 Jan MOS	S0	16.82	6328	-17.8	123(25)	1.08
HCG32A	2001 Jan MOS	E	14.93	12422	-21.2	238(13)	2.13
HCG32B	2001 Jan MOS	S0	16.11	12305	-20.0	219(15)	2.11
HCG32D	2001 Jan MOS	S0	16.51	12247	-19.6	231(11)	2.10
HCG40A	2001 Jan MOS	E	13.77	6604	-21.0	232( 6)	1.13
HCG40B	2001 Jan LS	S0	15.02	6690	-19.7	217(22)	1.15
HCG42A	2000 Apr MOS	E	12.08	3792	-21.4	291(30)	0.65
HCG42C	2000 Apr MOS	E	14.24	4045	-19.4	157(34)	0.69
HCG62:ZM19	2000 Apr LS	E	15.27	4204	-18.5	209(22)	0.72
HCG86A	2000 Apr MOS	E	13.97	5955	-20.5	292(12)	1.02
HCG86B	2000 Apr MOS	E	14.80	5817	-19.6	248(17)	1.00
<b>Spiral Bulges</b>							
HCG4A	2001 Jan MOS	SBbc	14.16	8042	-21.0	83(20)	1.38
HCG14A	2001 Jan MOS	Sa	14.44	5977	-20.1	93(11)	1.02
HCG14B	2001 Jan MOS	Sa	14.77	5386	-19.5	134(29)	0.92
HCG16A	2001 Jan MOS	Sb	12.91	4032	-20.7	147(50)	0.69
HCG16B	2001 Jan MOS	Sa	13.73	3876	-19.8	171(32)	0.67
HCG22B	2001 Jan MOS	Sa	15.47	2663	-17.3	76(31)	0.46
HCG25B	2001 Jan MOS	SBa	15.21	6334	-19.4	134(18)	1.09
HCG40D	2001 Jan MOS	SOa	15.06	6760	-19.7	141(25)	1.16
HCG62:ZM22	2001 Jan LS	Sc	15.36	4843	-18.7	114(16)	0.83

**Table 2.** Galaxy properties for both observing runs. Galaxy types are averages of values given in Hypercat. Total B magnitudes are from Paturel *et al.* (2000) if available and from NED if not. Absolute magnitudes are calculated from the estimated recession velocity assuming  $H_0 = 75$  km/s/Mpc. Recession velocities and velocity dispersions are estimated from our spectra. Velocity dispersion errors are given in brackets. Recession velocities are *not* heliocentric velocities but rather *observed* velocities. The effective aperture size is calculated according to Jørgensen *et al.* (1995).

applied to the velocity dispersion corrected indices and the error in the mean added in quadrature to index errors for the purposes of SSP fitting (Section 5).

Comparison of  $Mg_2$  index measurements with values published in Hypercat are shown in Fig. 2. Data in this plot are all aperture corrected according to Jørgensen (1997). Only  $Mg_2$  is compared as no other indices have been reported in previous studies that include HCGs common to this work. Agreement can be seen to be reasonably good, although the scatter is slightly larger than the errors. The cause of this scatter is unknown. However, it should be noted that  $Mg_2$  is one of  $\sim 20$  indices used in the derivations of age and metallicity detailed in Section 5. Consequently, the effects on this (or any other) individual index on the final age/metallicity determinations is expected to be small.

## 4.2 Correlations with velocity dispersion

The trends of various indices with velocity dispersion are shown in Fig. 3. The thin line shown in the  $Mg_2$  plot is the correlation reported by Bernardi *et al.* (1998). Thin lines in the remaining plots are from the data of Kuntschner (2000) for Fornax cluster galaxies (after conversion of line indices to a linear index scale and aperture correction). The thick lines are relations for spiral galaxy bulges from PS02 (after aperture correction). While there are small off-sets evident in some indices (most noticeably  $\langle Fe \rangle$ ), agreement with the previously published correlations are generally good.

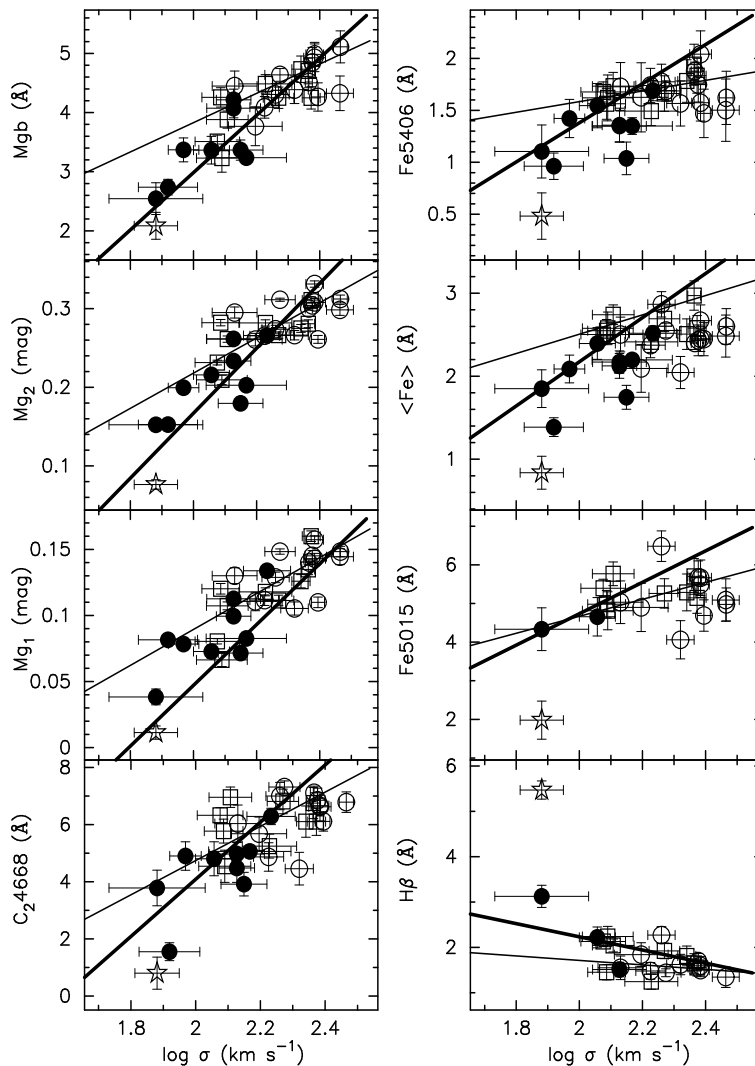


**Figure 3.** Index–velocity dispersion relations are shown. Elliptical galaxies are shown by open circles, S0s by open squares and spiral bulges by filled circles. The starburst galaxy (HCG16X) is marked by a star symbol. Data have been aperture corrected according to the prescription in Appendix A of Jørgensen (1997). The thin line in the  $Mg_2$  plot shows the relation for elliptical and S0 galaxies from Bernardi *et al.* (1998). This samples includes 931 field, group and cluster galaxies. Thin lines in the remaining plots are the Fornax E/S0 relations from Kuntschner (2000) (after conversion of line indices to a linear index scale and aperture correction). Thick lines in all plots are the PS02 relations for spiral galaxy bulges (after aperture correction). Although not identified separately, Arp-Madore galaxies and those in the NGC 5044 loose group follow the same general trends as HCG galaxies.

### 4.3 Emission

A plot of  $H\beta$  against Fe5015 is shown in Fig. 4. Both of these indices are susceptible to emission. It is clear from this diagram that a number of galaxies fall below the grids. This is consistent with the presence of emission in these galaxies. However, for galaxies lying just below the grids it *might* reflect an overestimation of  $H\beta$  in the SSPs. Unfortunately, it was not deemed possible to estimate emission by the procedure of measuring [OIII]5007 (Gonzalez 1993) due to the relatively low signal-to-noise of the data and the small number of suitable template stars observed. The identification and handling of these emission affected indices was therefore carried out by consideration of *all* indices in a galaxy. This procedure is described in the Section 5.

## 5 DETERMINATIONS OF AGE, METALLICITY AND ABUNDANCE RATIOS

This section details the estimation of age,  $[Fe/H]$  and  $[E/Fe]$ , where  $[E/Fe]$  is the abundance ratio of enhanced elements; C,O, Mg etc to Fe (see PS02). To facilitate comparison of results to the studies of T00, and PS02, determinations of  $\log(\text{age})$ ,  $[Fe/H]$  and  $[E/Fe]$  (hereafter; derived parameters) were carried out using Vazdekis (1999) single stellar populations (SSPs) and Tripicco & Bell (1995) index sensitivities, as described in PS02<sup>\*</sup>. Briefly, each index in the

<sup>\*</sup> T00 in fact used Worthey (1994) SSPs and a slightly different method of estimating derived parameters. However, these differences in combination result in values that differ by amounts similar to the quoted errors.

Index	Units	Lick - our value	Error in mean	Lick rms per obs.
H $\delta_A$	Å	0.229 ± 0.599	0.226	0.64
H $\delta_F$	Å	-0.153 ± 0.429	0.162	0.40
CN <sub>1</sub>	mag	-0.014 ± 0.041	0.013	0.02
CN <sub>2</sub>	mag	-0.012 ± 0.012	0.004	0.02
Ca4227	Å	-0.089 ± 0.171	0.060	0.27
G4300	Å	-0.489 ± 0.251	0.079	0.39
H $\gamma_A$	Å	-0.253 ± 0.432	0.153	0.48
H $\gamma_F$	Å	-0.118 ± 0.183	0.064	0.33
Fe4383	Å	-0.015 ± 0.542	0.192	0.53
Ca4455	Å	0.070 ± 0.437	0.155	0.25
Fe4531	Å	-0.382 ± 0.258	0.091	0.42
C4668	Å	-0.839 ± 0.270	0.095	0.64
H $\beta$	Å	-0.052 ± 0.153	0.048	0.22
Fe5015	Å	-0.104 ± 0.295	0.104	0.46
Mg <sub>1</sub>	mag	0.016 ± 0.012	0.004	0.01
Mg <sub>2</sub>	mag	0.023 ± 0.011	0.003	0.01
Mgb	Å	0.024 ± 0.135	0.043	0.23
Fe5270	Å	-0.324 ± 0.286	0.090	0.28
Fe5335	Å	-0.394 ± 0.243	0.077	0.26
Fe5406	Å	-0.181 ± 0.127	0.045	0.20
Fe5709	Å	-0.030 ± 0.147	0.052	0.18
Fe5782	Å	0.045 ± 0.126	0.045	0.20
Na D	Å	-0.097 ± 0.200	0.063	0.24
TiO <sub>1</sub>	mag	0.003 ± 0.007	0.002	0.01
TiO <sub>2</sub>	mag	-0.008 ± 0.005	0.002	0.01

**Table 3.** Offsets from our index measurements to those of the Lick system. Mean offset and scatter about the mean for 6 Lick standard stars observed during both 2000 and 2001 runs are given. Error in the mean is also given. This error must be added in quadrature to errors in Tables A1 to A4 prior to age/metallicity determinations. Also given is the typical rms error per observation of the Lick calibrators (see Worthey *et al.* 1994).

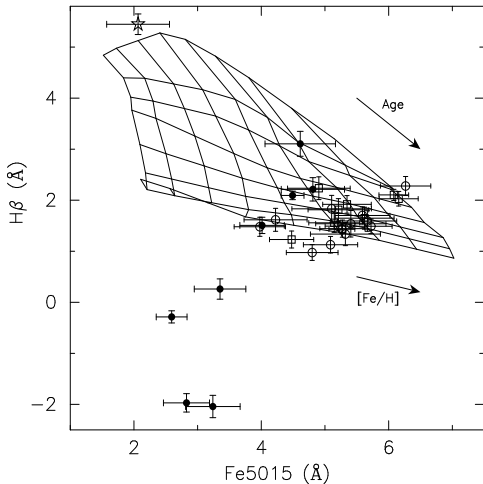


**Figure 4.** Plot of H $\beta$  against Fe5015. Symbols as in Fig. 3. Grid lines represent lines of constant [Fe/H] (from -1.5 to +0.5 dex in 0.25 dex steps) and age (1, 1.5, 2, 3, 5, 8, 12 and 17 Gyr; bottom line) for solar abundance ratio SSPs. The plot shows the effects of emission on these indices in some galaxies i.e. they lie below the grids. One galaxy (HCG4A) with both Fe5015 and H $\beta$  of  $\sim -5$  Å has been omitted from this plot.

model SSPs was interpolated to give a grid of values for  $-1 < \log(\text{age}) < 1.25$  dex and  $-1.675 < [\text{Fe}/\text{H}] < 0.5$  dex in 0.025 dex steps. For each index, at each  $\log(\text{age})$ , [Fe/H] step, values of the index were also estimated for  $-0.3 < [\text{E}/\text{Fe}] < 0.6$  dex, again in 0.025 dex steps. These enhanced values were estimated by assuming an appropriate (55%/44%/3%) mix of the three stellar types whose index sensitivities were modeled by Tripicco & Bell (1995). The elements C, N, O, Mg, Na and Si were assumed to be in the enhanced group (i.e. E in [E/Fe]), while Fe, Ca and Cr were taken to be Fe peak elements. The fractional change in each index was then calculated by assuming that all elements in the enhanced group vary by the same amount when compared to the Fe peak elements. In this way a three dimensional grid (with axes;  $\log(\text{age})$ , [Fe/H] and [E/Fe]) was generated for each index. The procedure used for estimating the derived parameters then involved simultaneously finding the best fit (by  $\chi^2$  minimisation) of as many observed indices as possible ( $\sim 20$ ) to the three dimensional grids of model indices.

The rationale for using a large number of indices (rather than the 3 or 4 often used, e.g. Kuntschner *et al.* 2001; Kuntschner *et al.* 2002; Caldwell, Rose & Concannon 2003; Mehlert *et al.* 2003; Denicolo *et al.* 2003) was arrived at in the following way: While each index is, to some degree, sensitive to each of the derived parameters, the various degeneracies makes their estimation from individual indices impossible. As well as errors in observations and reductions, we must also consider the large number of uncertainties in the modeling (comparison of complex populations to SSPs, errors in the SSP grids themselves and the rather crude models of the effects of relative abundances). However, despite these difficulties, it remains true that each index does contain *some* information on each of the derived parameters. PS02 therefore postulated that, if a sufficiently large number of indices were employed it may be possible to extract this information with acceptable accuracy. In order to test this hypothesis, PS02 used various combinations of indices to estimate derived parameters, including estimates with all Balmer lines excluded from the fitting procedure, i.e. *using only metallicity sensitive indices*. The more common combinations of 3 or 4 indices were also tested. The estimates of derived parameters from the various combinations of indices were shown to be in good agreement with only moderate scatter ( $\sim 0.1$  dex) about values obtained using all indices (see table 11 of PS02). PS02 therefore concluded that *ages and metallicities can be derived without the use of Balmer lines if a sufficiently large number of indices are included in the fitting procedure*.

Given these considerations, the use of a large number of indices would seem to have several distinct advantages;

- The procedure is particularly useful in spectra that are not emission corrected, as affected indices can be identified and omitted from the determination (see below) with only a modest increase in errors.
- Derived parameters are less prone to reduction errors, e.g. flux calibration error, stray cosmic rays, skyline residuals, velocity dispersion error, errors in conversion to the Lick system, etc.
- Derived parameters are less prone to modeling errors in individual indices.

While the process of estimating derived parameters

used here is based on that in PS02, there were some minor differences in methodology. Firstly, the molecular band indices were assumed to have an *additive* Tripicco & Bell (1995) correction (in line with Thomas et al. 2003). In addition, Ti was included amongst the enhanced elements for the application of Tripicco & Bell (1995). These modifications to the PS02 procedure make only small differences to the derived parameters. More importantly, due to the presence of emission affected indices and the signal-to-noise of our data, certain indices were ‘clipped’ from the fitting process using the following procedure. Initially the best fit age/[Fe/H]/[E/Fe] were estimated with (the emission affected) Balmer lines and Fe5015 excluded from the fitting procedure. Deviations of the observed Balmer lines and Fe5015 from the best fit SSP values were then considered, and indices whose observed value deviated by more than  $3\sigma$  from the best fit SSP value were deemed to be suffering from emission. These indices were then permanently excluded from the fitting process. A  $3\sigma$  offset in  $H\delta_A$ ,  $H\delta_F$ ,  $H\gamma_A$ ,  $H\gamma_F$  and  $H\beta$  (with typical errors of  $\sim 0.4$ ,  $0.3$ ,  $0.4$ ,  $0.3$  and  $0.2 \text{ \AA}$  respectively) corresponds to  $\log(\text{age})$  differences of  $\sim 0.25$ ,  $0.45$ ,  $0.25$ ,  $0.35$  and  $0.5$  dex. The clipping procedure therefore only excludes indices when derived parameter estimates obtained from the remaining indices differ significantly from that implied by the clipped index.

Once emission affected indices had been eliminated, another fit to SSP values was obtained, this time using all remaining indices. Again indices were clipped, this time using a  $5\sigma$  limit. The  $5\sigma$  clipping process was iterated (if necessary) until a fit was obtained in which no index deviated from best fit SSP values by more than  $5\sigma$ . In fact only one galaxy (HCG86A) required a second iteration. All but one of the 5 indices clipped at this stage were found (by visual inspection) to be affected by sky-line residuals.

The final fit (with no indices deviating by more than  $5\sigma$ ) was taken as giving the final values. Indices affected by vignetting and those clipped from the fitting procedure have been omitted from Tables A1 to A4. The values of the derived parameters are given in Table B1 with subscript *raw*. This is to indicate that there are two further corrections that must be applied before values are fully calibrated.

The first correction relates to local abundance trends, as the values of  $[E/Fe]_{raw}$  given in Table B1 are enhancements with respect to the stellar calibrators used in the construction of the SSPs. These stars were selected from the solar neighbourhood and therefore possess an inherent [E/Fe] that varies with [Fe/H] (e.g. Edvardsson et al. 1993; Gustafsson et al. 1999; Bensby, Felzing & Lundstrom 2003).

In order to understand the need for the local abundance ratio pattern correction, consider a galaxy, the observed spectra of which give derived parameters;  $[E/Fe]_{raw}=0.0$  and  $[Fe/H]=-0.5$ . This is equivalent to saying that the observed spectrum is best matched by the SSP with  $[Fe/H]=-0.5$ , *without* the need to adjust indices using the Tripicco & Bell (1995) abundance ratio sensitivities.

Now, the stellar library used to construct the SSP is composed of stars in the solar neighbourhood, and therefore reflect the local abundance ratio pattern. Thus the SSP at  $[Fe/H]=-0.5$  is generated using stars with an [E/Fe] of  $\sim +0.25$  dex (see, for example, Bensby, Feltzing & Lundstrom 2003). Therefore, given that the galaxy spectrum is best matched by the *unadjusted*  $[Fe/H]=-0.5$  SSP, we must

conclude that the SSP and the galaxy have the same [E/Fe] of  $+0.25$  dex.

This example can be generalised by considering the value  $[E/Fe]_{raw}$  to represent the offset between [E/Fe] in the galaxy and [E/Fe] in the best fit SSP. Finally, it should be noted that solar neighbourhood stars (and consequently the SSPs) with  $[Fe/H]>-1.0$  have [E/Fe] that varies with [Fe/H]. This variation (see, for example, Bensby, Feltzing & Lundstrom 2003) can be approximated by;

$$[E/Fe] = -0.5[Fe/H]. \quad (1)$$

The correction for the local abundance ratio pattern therefore estimates the final value of [E/Fe] in galaxies with  $[Fe/H]>-1.0$  using;

$$[E/Fe]_{final} = -0.5[Fe/H] + [E/Fe]_{raw}. \quad (2)$$

This correction is clearly only approximate. A more accurate analysis must account for the variety of behaviours of elements within the E group with [Fe/H]. This issue will be addressed in future works.

In many previous works the correction outlined above is either omitted altogether (e.g. T00; Kuntschner et al. 2002) or applied only to galaxies with  $[Fe/H]<0$  (e.g. PS02; Thomas et al. 2003). However, recent studies of local stars have suggested that it should be applied to all galaxies with  $[Fe/H]>-1.0$ , including those with  $[Fe/H]>0$  (Felzing & Gustafsson 1998; Gustafsson et al. 1999; Bensby et al. 2003; see Appendix B). This is the procedure adopted in this paper. The data of T00 and PS02 have also been corrected to make them consistent with the HCG analysis. A more complete justification and detailed account of this correction are given in Appendix B.

The second correction that must be made to the raw values is that for the varying size of apertures within and between studies. This correction was carried out by the procedure described in Appendix A1.2 of Jørgensen (1997) using equation A2 and values  $\alpha=+0.2$  for  $[Fe/H]$ ;  $\alpha=0.0$  for [E/Fe]; and  $\alpha=-0.04$  for  $\log(\text{age})$ . These values were estimated from gradients in derived parameters found in Proctor (2002).

The final derived parameters (corrected for both aperture and local enhancement trends) are given in Table B1 with the subscript *corr*. It is these values upon which the following analysis is based. Values of [E/H] (where  $[E/H]=[E/Fe]+[Fe/H]$ ) are also given in this table. [E/H] is used here, rather than the more commonly quoted [Z/H], as this aids in consideration of the correlations and temporal evolution of the two element groups of interest. However, the difference between [E/H] and [Z/H] is less than 0.04 dex for all galaxies in the sample.

## 6 RESULTS AND DISCUSSION

The results presented in this section are fully corrected to the Lick system. This includes both aperture correction and correction for the local abundance trends (see Appendix B). Plots include the measurements from T00 and PS02 data sets. From the present study we show results for 17 early-type galaxies and 9 spiral bulges in HCGs and 6 early-type galaxies in groups or the field. The T00 sample includes 49 early-type galaxies of which 11 are in the Fornax cluster,

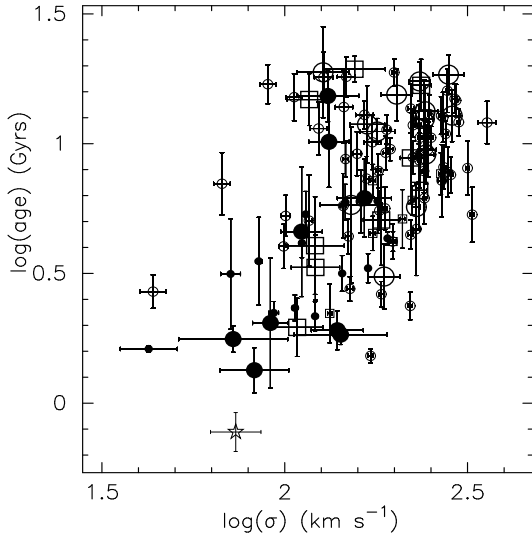


**Figure 5.** Plots of  $\log(\text{age})$  with  $\log \sigma$  for galaxies in the current sample (large symbols) as well as T00 and PS02 samples (small symbols). Symbols are otherwise the same as Fig. 3.

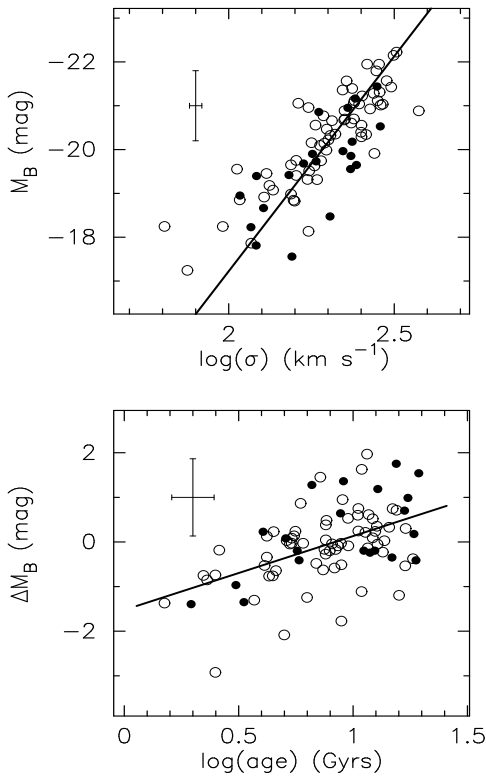


**Figure 6.** The top figure shows the Faber-Jackson relation (Faber & Jackson 1976) for 88 early-type galaxies in the three samples. Galaxies in the current work are shown as solid symbols. The solid line is the relation from Forbes & Ponman (1999). Error bars represent an average error in  $\log(\text{age})$ , while errors in  $M_B$  and  $\Delta M_B$  are those which result from an assumed error of  $350 \text{ km s}^{-1}$  (see text for details). Reasonable agreement is found with Forbes & Ponman relation. The bottom plot shows residuals to the Faber-Jackson relation plotted against  $\log(\text{age})$ . The line shows the least-squares fit to the data. This correlation has a  $>99.99\%$  significance.

8 are in the Virgo cluster and 30 are in low density environments (groups and field). NGC 221 and NGC 224 have been omitted from the original T00 sample due to the large aperture corrections required for such nearby galaxies. The PS02 sample includes 6 Virgo cluster early-type galaxies, 2 galaxies in HGC68 (NGC 5353 and NGC 5354), 9 early-type galaxies in loose groups and the field as well as 15 spiral bulges. The combined sample therefore contains 89 early-type galaxies and 24 spiral bulges, in a variety of environments.

### 6.1 Correlations for early-type galaxies

A plot of luminosity-weighted age against velocity dispersion for the combined data sets (Fig. 5) indicates that the galaxies in the three samples exhibit a large range of ages. The plot also indicates a trend between age and velocity dispersion for both E/S0s and spiral bulges. Such a trend for early-type galaxies is also evident in other studies (e.g. Caldwell *et al.* 2003; Denicolo *et al.* 2003; Mehlert *et al.* 2003). However, some care must be taken when interpreting this figure as old, low velocity dispersion (i.e. low luminosity) galaxies, which could populate the top left quadrant of the plot may be excluded from any sample by signal-to-noise limitations.

The broad range of ages found in the E/S0 galaxies of these studies permits testing of the Forbes & Ponman (1999) finding of a correlation between the residual of the Faber-Jackson relation and age. A plot of the Faber-Jackson relation for the data in the two studies is shown in Fig. 6. Values of  $M_B$  were calculated using published distances to Virgo and Fornax clusters (16.8 and 18.4 Mpc respectively). However, for HCG and field galaxies, distances were calculated using simply recession velocities (a Hubble constant of  $75 \text{ km s}^{-1} \text{ Mpc}^{-1}$  is assumed throughout). Fig. 6 (upper) shows that the relation given in Forbes & Ponman (1999) is reproduced with a rms scatter  $\sim 0.8$  mag. This scatter is equivalent to an uncertainty in distance estimates characterised by a recession velocity of only  $350 \text{ km s}^{-1}$ , well within the random velocities of the field and group galaxies with respect to the Hubble flow. In the plot of residuals to the Faber-Jackson relation against age (lower plot) a correlation is also found with confidence  $>99.99\%$ . This supports the Forbes & Ponman (1999) finding and gives us confidence that the age/metallicity degeneracy has indeed been broken in these studies.

Fig. 7 shows  $[\text{Fe}/\text{H}]$  and  $[\text{E}/\text{Fe}]$  (and their sum  $[\text{E}/\text{H}]$ ) for early-type galaxies in the three studies, plotted against velocity dispersion and age. Bearing in mind that 89 galaxies are plotted in each of these figures, strong correlations of both  $[\text{Fe}/\text{H}]$  and  $[\text{E}/\text{H}]$  with age are evident. Fits were obtained (by least-squares fitting) to each of these relations. These are shown in Fig. 7 as solid lines. The fits were obtained using the field/loose group galaxies only, as these galaxies; i) span the largest ranges in both age and  $\log$  velocity dispersion; ii) constitute over 50% of the combined sample; and iii) this environment was sampled in all three studies. The correlations shown in Fig. 7 are consistent with the results of PS02 and T00 (once differences in the applied correction for local abundance trends have been accounted for), and are also evident in the HCG data alone. Thus we find age-metallicity and age-abundance ratio re-



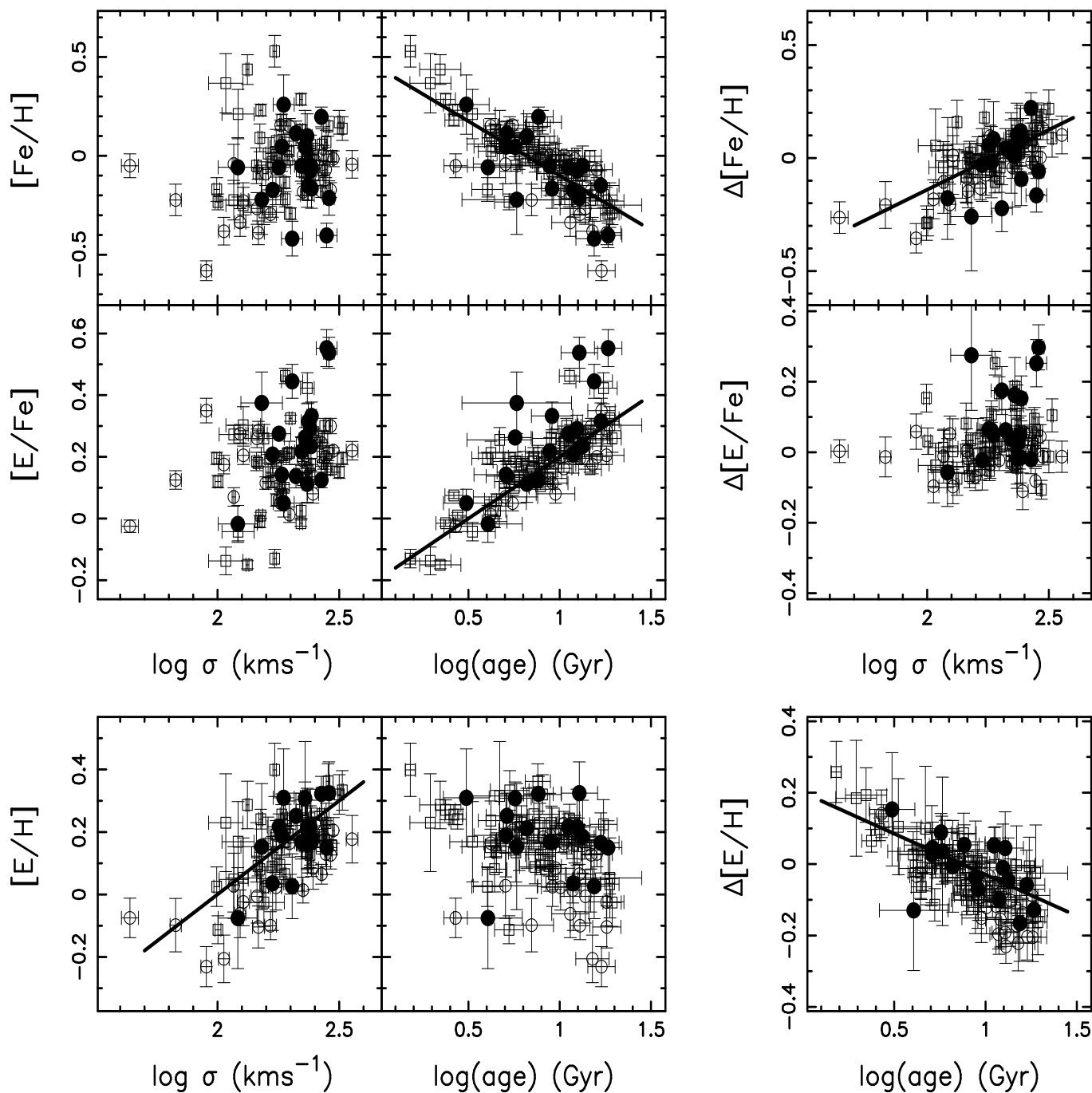


**Figure 7.** Plot of fully corrected derived parameters against  $\log \sigma$  and  $\log(\text{age})$  (left-hand plots). Data from this study, T00 and PS02 are shown. HCG galaxies are shown as filled circles, while cluster galaxies are shown as open circles and those in loose groups and the field as open squares. Lines are the correlations identified in the text. Strong correlations are evident in both  $[\text{Fe}/\text{H}]$  and  $[\text{E}/\text{Fe}]$  with  $\log(\text{age})$ , while, for  $[\text{E}/\text{H}]$  the strongest correlation is with  $\log \sigma$ . Residuals to these correlations are shown on the right. For  $[\text{Fe}/\text{H}]$  and  $[\text{E}/\text{H}]$  weak correlations also exist with  $\log \sigma$  and  $\log(\text{age})$  respectively.

lations which indicate that older galaxies are more Fe poor and  $\alpha$ -element enhanced than younger galaxies.

For  $[\text{E}/\text{H}]$ , the strongest correlation is with velocity dispersion. This clearly indicates that while  $[\text{Fe}/\text{H}]$  and  $[\text{E}/\text{Fe}]$  are primarily dependent on age there is also some dependence on velocity dispersion. Fig. 7 also shows the residuals of fits to the correlations identified above (estimated by least squares fitting). It is evident from these plots that residu-

als to the  $[\text{Fe}/\text{H}]$ – $\log(\text{age})$  relation correlate with  $\log \sigma$ , while residuals to the  $[\text{E}/\text{H}]$ – $\log \sigma$  relation correlate with  $\log(\text{age})$ . There is also a suggestion that the residuals to the  $[\text{E}/\text{Fe}]$ – $\log(\text{age})$  relation correlate with  $\log \sigma$ , but this correlation is not statistically significant. It is also clear from the residuals in Fig. 7 that HCGs generally follow the field galaxy correlations reasonably well, albeit with a tendency for some HCG galaxies to exhibit lower  $[\text{Fe}/\text{H}]$  residuals and higher  $[\text{E}/\text{Fe}]$

residuals than both field and cluster galaxies. However, these galaxies exhibit some of the highest  $\alpha$ -enhancements in the combined sample. The offsets in residuals in these galaxies may then simply indicate limitations in the modeling process rather than real differences. It therefore seems unwise to draw any conclusions from these galaxies.

Given the dependence of  $[\text{Fe}/\text{H}]$ ,  $[\text{E}/\text{Fe}]$  and  $[\text{E}/\text{H}]$  on both age and velocity dispersion, and the similarity of the galaxies in all environments, full three dimensional fits of the form  $[\text{Fe}/\text{H}] = \alpha \log(\text{age}) + \beta \log(\sigma) + \gamma$  were found to the whole galaxy sample (see also T00). These fits gave;

$$[\text{Fe}/\text{H}] = -0.60 \log(\text{age}) + 0.65 \log \sigma - 1.00 \quad (3)$$

$$[\text{E}/\text{Fe}] = 0.30 \log(\text{age}) + 0.05 \log \sigma - 0.20 \quad (4)$$

$$[\text{E}/\text{H}] = -0.25 \log(\text{age}) + 0.60 \log \sigma - 1.00 \quad (5)$$

Equations 3 to 5 indicate that the gradients of  $[\text{Fe}/\text{H}]$  and  $[\text{E}/\text{H}]$  with age differ significantly, with the rate of Fe evolution approximately twice that of elements in the enhanced group. On the other hand, it is evident that the gradients of  $[\text{Fe}/\text{H}]$  and  $[\text{E}/\text{H}]$  with velocity dispersion are almost identical. This is a result of finding only a statistically insignificant correlation between  $[\text{E}/\text{Fe}]$  and velocity dispersion. This result is in stark contrast to the findings of many previous studies, including Trager *et al.* (2000) and PS02, the data from which have been re-analysed here. The discrepancy between the findings of this work and the previous studies is the result of differences in the local abundance ratio correction applied in each study (see Appendix B). This emphasises the importance of this (often overlooked) correction. The lack of correlation between  $[\text{E}/\text{Fe}]$  and velocity dispersion is interesting in the context of galaxy formation models, as the ‘semi-cosmological’ N-body-SPH models of Kawata (Kawata 2001; Kawata & Gibson 2003), which model the hierarchical formation of individual galaxies, fail to reproduce a correlation between  $[\text{E}/\text{Fe}]$  and velocity dispersion, while the N-body-SPH monolithic collapse models of Pipino & Matteuchi (2003) require gas infall timescales that anti-correlate with galaxy mass in order to reproduce the assumed correlation. This again underlines the importance of the local abundance ratio corrections required to fully calibrate the derived parameters.

In order to investigate possible variations in the derived parameters with environment we divided the sample into four categories; clusters, massive groups, HCGs and finally small groups/field. Cluster galaxies are those in Virgo and Fornax from T00 and PS02. Massive group galaxies include those in the NGC 5044 group and all other galaxies identified as having at least 10 neighbours in Garcia (1993). All remaining galaxies not in HCGs were attributed to the small group/field category. Galaxies with  $\log \sigma \leq 2.075$  were omitted from this analysis to ensure that the mass distribution in the different environments were as similar as possible. Averages of  $\log \sigma$  and the derived parameters for galaxies in each environment are presented in Table 4. Errors in the mean are also presented. The mean velocity dispersion and its range can be seen to be almost identical in the four environments. Table 4 also indicates that galaxies in low density environments (small groups/field) exhibit a lower average age (5.9 Gyr) than those in clusters (11.0 Gyr) and massive groups (10.2 Gyr). This is consistent with the results of pre-

vious authors (e.g. Rose *et al.* 1994; Kuntschner *et al.* 2002; Terlevich & Forbes 2002). It is also qualitatively consistent with the predictions of hierarchical formation models (e.g. Baugh, Cole & Frenk 1996; Kauffmann & Charlot 1998).

Galaxies in low density environments also appear to possess higher  $[\text{Fe}/\text{H}]$  than their cluster and massive group counterparts. This is again consistent with the findings of Rose *et al.* (1994). In order to test the effect of differences in the morphological mix (elliptical to S0) in each of the samples, average values of derived parameters were also calculated for elliptical galaxies only. No significant qualitative differences in the results shown in Table 4 were observed.

Comparison of HCG galaxies to galaxies in other environments (Table 4) therefore shows them to possess distributions of derived parameters more in keeping with those of galaxies in high density environments than those of galaxies in small groups and the field, i.e they are on average older and possess higher  $[\text{Fe}/\text{H}]$  than their low density environment equivalents. This is consistent with the findings of de la Rosa *et al.* (2001b) who also found such a difference in age and metallicity. However, the five early-type galaxies that are the brightest in their respective compact groups (i.e. HCG22A, HCG32A, HCG40A, HCG42A, HCG86A and HCG68A from PS02) have an average  $\log(\text{age})$  of  $1.03 \pm 0.07$  dex ( $10.7 \pm 1.9$  Gyr). This is *older* than the average of the HCG sample as a whole, with the remaining galaxies having an average  $\log(\text{age})$  of  $0.89 \pm 0.07$  dex ( $7.7 \pm 1.4$  Gyr). These findings contradict the prediction of the Kauffmann (1996) hierarchical formation models that the brightest galaxies in such groups should be the youngest. However, they are, at least qualitatively, consistent with the Chiosi & Carraro (2002) models of monolithic collapse, although these models do not appear to be able to explain the extremely young ages observed in some galaxies.

## 6.2 Correlations for spiral bulges

The HCG data for spiral bulges are in good agreement with PS02 in that they exhibit lower average ages than early-type galaxies and show strong correlations of both  $[\text{Fe}/\text{H}]$  and  $[\text{E}/\text{H}]$  with  $\log \sigma$  (Fig. 8). The gradient of the  $[\text{E}/\text{H}]$ - $\log \sigma$  correlation in spiral bulges (0.65 dex/dex) is similar to that found in early-type galaxies (Equation 5). Indeed, combined  $[\text{E}/\text{H}]$ - $\log \sigma$  plots of spiral bulges and early-type galaxies show a single overlapping relation (see Fig. B2). However, the gradient of the  $[\text{Fe}/\text{H}]$ - $\log \sigma$  correlation in bulges (1.0 dex/dex) appears to differ from that in early-types (0.65 dex/dex). No correlations were found among the residuals to these correlations. Fig. 8 also indicates no significant differences in  $\log(\text{age})$ ,  $[\text{Fe}/\text{H}]$  or  $[\text{E}/\text{Fe}]$  between spiral bulges in HCGs and those in other environments. We note that Proctor (2002) showed that, even in edge-on systems, disc contamination was below 10%, in the central regions of spiral bulges. Disc contamination is therefore not considered significant in this study.

## 7 CONCLUSIONS

We have investigated the ages, metallicities and abundance ratios of galaxies in a variety of environments and compared them to those of Hickson Compact Group galaxies. It has

Environment	N	Average log $\sigma$	Average log(age)	Average [Fe/H]	Average [E/Fe]
HCG	18	2.32(0.02)	0.93(0.05)	-0.07(0.04)	0.26(0.04)
Cluster	20	2.32(0.03)	1.04(0.03)	-0.11(0.03)	0.19(0.02)
Massive Group	13	2.34(0.04)	1.01(0.05)	-0.07(0.03)	0.25(0.03)
Small group/field	30	2.28(0.02)	0.77(0.05)	0.07(0.03)	0.12(0.02)

**Table 4.** The average values of derived parameters for E/S0 galaxies in the combined sample are given by environment. Errors in the mean are given in brackets. Galaxies with  $\log \sigma < 2.075$  are omitted to ensure a close match in  $\log \sigma$  distributions in the four environments. HCG galaxies can be seen to more closely resemble cluster/massive group galaxies than those in small groups/field. No qualitative differences were observed when only elliptical galaxies were considered.

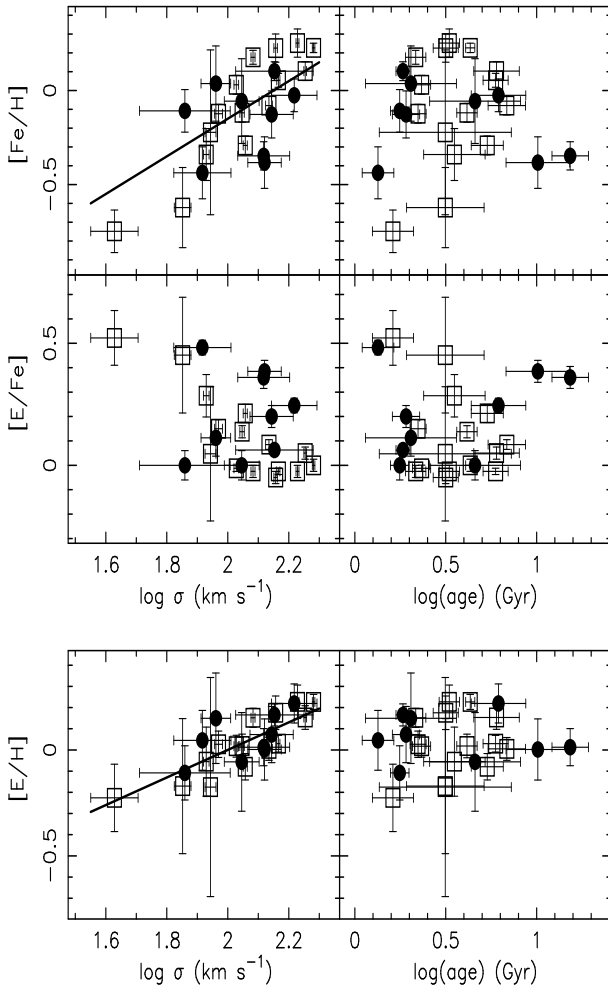


**Figure 8.** Plots of metallicity parameters in spiral bulges against  $\log(\text{age})$  and  $\log \sigma$ . Best fit lines (least squares fitting) are shown for [Fe/H] and [E/H] against  $\log \sigma$ . Spiral bulges in HCGs are shown as filled circles, while those in all other environments are shown as open squares.

been shown that early-type galaxies in all environments exhibit a range of ages. Residuals to the Faber-Jackson relation correlate reasonably well with age in all environments, consistent with Forbes & Ponman (1999) and giving confidence that the age/metallicity degeneracy has been broken.

Correlations were detected between age and velocity

dispersion in both early- and late-type galaxies, with high velocity dispersion galaxies exhibiting older ages. This is, at least qualitatively, consistent with previous studies as well as the monolithic collapse models of Chiosi & Carraro (2002). However, studies must be extended to lower velocity dispersions to confirm this finding.

The distributions of age in the various environments (HCGs, clusters, massive groups and small groups/field) confirmed the prediction of hierarchical formation models (e.g. Baugh *et al.* 1996; Kauffmann & Charlot 1998) and the findings of previous studies (e.g. Kuntschner *et al.* 2002; Terlevich & Forbes 2002) that galaxies in the field have a lower average age than those in clusters. However, the finding that HCGs more closely resemble cluster galaxies than those in the field is inconsistent with current hierarchical formation models. The brightest galaxies in HCGs were also shown to be *older* than their less luminous companions. This is in stark contrast with the Kauffmann (1996) prediction that the brightest galaxies in such groups should be younger than their less luminous neighbours.

Our study also confirmed the previously reported finding (de la Rosa *et al.* 2001b) that early-type galaxies in HCGs are more metal poor than field galaxies. This again suggests that the star formation histories of early-type galaxies in HCGs more closely resemble those of cluster galaxies than those in less dense environments such as small groups and the field.

Metallicities (given by [Fe/H] and [E/H]) were found to show strong correlations with both age and velocity dispersion for early-type galaxies in all environments. These correlations were shown to be consistent across all galaxy environments. The correlations of [Fe/H] and [E/H] with age were shown to differ significantly in that Fe abundance exhibits a rate of change approximately twice that of the  $\alpha$ -elements in the enhanced group. However, the [Fe/H] and [E/H] correlations with velocity dispersion have similar gradients, as we find no significant correlation between  $\alpha$ -element enhancement ratio ([E/Fe]) and velocity dispersion. We therefore conclude that this correlation, that has been reported in many previous studies, is probably the result of a failure to fully calibrate the derived parameters to the Lick system. Specifically, the estimated values of [E/Fe] must be corrected for the pattern of [E/Fe] with [Fe/H] found in the local stars used to calibrate the Lick system.

Spiral bulges were shown to exhibit the same strong correlations of [Fe/H] and [E/H] with  $\log \sigma$  found in PS02. The [E/H]- $\log \sigma$  relation in bulges was shown to be the

same as that in early-type galaxies. However, the [Fe/H]–log  $\sigma$  relations differ between early- and late-type galaxies. No correlations with age were identified. No evidence was found for variation of star formation histories in spiral bulges with environment. We therefore find that the star formation histories of the centres of spiral bulges differ significantly from those in the centres of early-type galaxies.

### Acknowledgments

This work is based on observations made on the NTT, which is operated by ESO. The authors acknowledge the data analysis facilities provided by IRAF, which is distributed by the National Optical Astronomy Observatories and operated by AURA, Inc., under cooperative agreement with the National Science Foundation. R.P. thanks the Royal Society for funding that supported this work.

### References

- Athanassoula E., Makino J., Bosma A., 1997, *MNRAS*, 286, 825
- Baugh C.M., Cole S., Frenk C.S., 1996, *MNRAS*, 283, 1361
- Bensby T., Felzing S., Lundström I., 2003, *A&A*, 410, 527
- Bernardi M., Renzini A., da Costa L.N., Wegner G., Alonso M.V., Pellegrini P.S., Rit C., Willmer C.N.A., 1998, *ApJ*, 508, 143
- Caldwell N., Rose J.A., Concannon K.D., 2003, *AJ*, 125, 2891
- Chiosi C., Carraro G., 2002, *MNRAS*, 335, 335
- Coziol R., Ribeiro A.L.B., de Carvalho R.R., Capelato H.V., 1998, *ApJ*, 493, 563
- de la Rosa I.G., de Carvalho R.R., Zepf S.E., 2001a, *AJ*, 122, 93
- de la Rosa I.G., Coziol R., de Carvalho R.R., Zepf S.E., 2001b, *ApSS* 276,717
- Diaferio A., Gell M.J., Ramella M., 1994, *AJ*, 107, 868
- Denicolo G., Terlevich R., Terlevich E., Forbes D., Terlevich A., 2003 in prep.
- Edvardsson B., Andersen J., Gustafsson B., Lambert D.L., Nissen P.E., Tomkin J., 1993, *A&A*, 275, 101
- Felzing S., Gustafsson B., 1998, *A&AS*, 129,237
- Faber S.M., Jackson R.E., 1976, *ApJ*, 204, 668
- Forbes, D., 1992, *A&AS*, 92, 583
- Forbes, D., Ponman, T., 1999, 309, 623
- Garcia A.M., 1993, *A&AS*, 100, 47
- de la Rosa I.G., Coziol R., de Carvalho R.R., Zepf S., 2001, *Ap&SS*, 276, 717
- González J.J., 1993, Ph.D Thesis, University of California, Santa Cruz
- Governato F., Tozzi P., Cavaliere A., 1996, *ApJ*, 458, 18
- Gustafsson B., Karlsson T., Olsson E., Edvardsson B., Ryde N., 1999, *A&A*, 342, 426
- Hernquist, L., Katz, N., Weinberg, S., 1995, *ApJ*, 442, 57
- Hickson P., 1982, *ApJ*, 255, 382
- Jones, L., Ponman, T., Forbes, D., 2000, 312, 319
- Jørgensen I., Franx M., Kjærgaard P., 1995, *MNRAS*, 276, 1341
- Jørgensen I., 1997, *MNRAS*, 288, 161
- Kauffmann G., 1996, *MNRAS*, 281, 487
- Kauffmann G., Charlot S., 1998, *MNRAS*, 294, 705
- Kawata D., 2001, *ApJ*, 558, 614
- Kawata D., Gibson B.K., 2003, *MNRAS*, 340, 908
- Kuntschner H., 2000, *MNRAS*, 315, 184
- Kuntschner H., Lucey J.R., Smith R.J., Hudson M.J., Davies R.L., 2001, *MNRAS*, 323, 615
- Kuntschner H., Smith R.J., Colless M., Davies R.L., Kaldare R., Vazdekis A., 2002, *MNRAS*, 337, 172 Mamon, G., 1986, *ApJ*, 307, 426
- Mehlert D., Thomas D., Saglia R.P., Bender R., Wegner G., 2003, *A&A*, 407, 423
- Mendes de Olivera C., Hickson P., 1994, 427, 684
- Nissen P.E., Edvardsson B., 1992, *A&A*, 261, 255
- Paturel G., Fang Y., Garnier R., Petit C., Rousseau J., 2000, *A&AS*, 146, 19
- Pipino A., Matteucci F., 2003, (in prep) Poggianti B.M., Bridges T.J., Mobasher B., Carter D., Doi M., Iye M., Kashikawa N., Komiyama Y., Okamura S., Sekiguchi M., Shimasaku K., Yagi M., Yasuda N., 2001, *ApJ*, 562, 689
- Ponman, T., Bourner, P., Ebeling, H., Bohringer, H., 1996, *MNRAS*, 283, 690
- Proctor R.N., 2002, Ph.D Thesis, University of Central Lancashire, Preston, UK (<http://www.star.uclan.ac.uk/~rnp/research.htm>)
- Proctor R.N., Sansom A.E., 2002, *MNRAS*, 333, 517 (**PS02**)
- Rose J.A., Bower R.G., Caldwell N., Ellis R.S., Sharples R.M., Teague P., 1994, *AJ*, 108, 2054
- Rubin, V., Hunter, D., Ford, W., 1991, *ApJS*, 76, 153
- Terlevich A.I., Forbes D.A., 2002, *MNRAS*, 330, 547
- Thomas D., Maraston C., Bender R., *MNRAS*, 339, 897
- Tovmassian, H., Tiersch, H., Martinez, O., Yam, O., 2000, *Small Galaxy Groups*, ed. M. Valtonen & C. Flynn, ASP Conference Series, Vol. 209, San Francisco
- Trager, S., Faber, S., Worthey, G., Gonzalez, J., 2000, *AJ*, 120, 165 (**T00**)
- Tripicco M.J., Bell R.A., *AJ*, 110, 3035 (**TB95**)
- Vazdekis A., 1999, [http://www.iac.es/galeria/vazdekis/](http://www.iac.es/galeria/vazdekis/Verdes-Montenegro, L., Yun M.S., Perea J., del Olmo A., Ho P.T.P., 1998, ApJ, 497, 89)
- White, S., 1990, *Dynamics and Interactions of Galaxies*, ed. R. Wielen, Heidelberg, Springer, p 380
- Worthey G., 1994, *ApJS*, 95,107 Worthey G., Ottaviani D.L., 1997, *ApJS*, 111, 377
- Worthey G., Faber S.M., González J.J., Burstein D., 1994, *ApJS*, 94, 687
- Zabludoff A.I., Mulchaey J.S., 1998, *ApJ*, 496, 39
- Zepf, S., Whitmore, B., 1991, *ApJ*, 383, 542

### APPENDIX A: LICK INDICES

The indices presented in Tables A1 to A4 are for the galaxies in the present study. Indices are fully corrected to the Lick system but *not* aperture corrected. Indices affected by vignetting effects and those clipped from the fitting procedure (see Section 5) are omitted.

### APPENDIX B: APERTURE AND ABUNDANCE RATIO CORRECTION

This section details the correction of derived parameters for the trends seen in the solar neighbourhood abundance ratios. Data from the studies of PS02 and T00 are included for

Galaxy	H $\delta_A$	H $\delta_F$	CN <sub>1</sub>	CN <sub>2</sub>	Ca4227	H $\gamma_A$	H $\gamma_F$	Fe4383	Ca4455	Fe4531	C <sub>2</sub> 4668
<b>Loose Group</b>											
NGC 3305	-3.121	-0.259	0.106	0.142	1.247	-6.886	-2.250	5.039	1.106	3.251	7.131
	0.352	0.228	0.008	0.010	0.142	0.285	0.181	0.344	0.179	0.256	0.360
NGC 5046	-3.316	-0.534	0.084	0.118	1.070	-7.191	-2.640	5.184	1.968	3.179	6.772
	0.655	0.429	0.015	0.018	0.261	0.523	0.337	0.607	0.296	0.447	0.648
NGC 5049	-3.264	-0.251	0.073	0.106	1.045	-6.776	-2.065	5.188	1.857	3.309	6.325
	0.412	0.266	0.010	0.011	0.166	0.332	0.210	0.389	0.192	0.285	0.418
<b>Field</b>											
NGC 2502	-2.508	-0.412	0.079	0.109	1.108	-7.984	-2.732	6.243	1.385	4.074	6.226
	0.465	0.307	0.011	0.013	0.179	0.366	0.232	0.399	0.205	0.294	0.419
NGC 3203	-1.681	0.103	0.051	0.082	1.110		-1.609	5.896	1.656	3.580	7.727
	0.345	0.228	0.008	0.010	0.141		0.177	0.329	0.170	0.250	0.356
NGC 6684	-1.740	0.251	0.049	0.077	1.079			5.664	1.344	3.277	7.660
	0.264	0.174	0.006	0.007	0.108			0.253	0.128	0.186	0.271
<b>Compact Group</b>											
HCG4C	-0.573	0.910	0.052	0.095	1.004	-5.841	-1.119	5.772	1.792	3.358	6.630
	0.422	0.278	0.010	0.012	0.191	0.369	0.228	0.439	0.220	0.328	0.478
HCG16X									0.321	1.214	0.858
									0.248	0.371	0.562
HCG22A	-2.905	-0.319	0.105	0.144	1.244	-6.904	-2.098	5.691	1.362	3.177	8.084
	0.232	0.152	0.005	0.006	0.092	0.180	0.114	0.201	0.104	0.151	0.215
HCG22D		-0.038	0.075	0.113	1.303	-6.687	-2.261	4.919	1.841	2.461	6.104
		0.322	0.012	0.014	0.203	0.392	0.251	0.467	0.234	0.439	0.479
HCG22E					0.946	-6.361	-1.592	5.080	1.270	2.875	4.856
					0.200	0.383	0.239	0.453	0.230	0.332	0.498
HCG22X	-2.147	-0.145	0.079	0.121	1.409	-7.700	-2.375	5.137	1.561	3.542	6.624
	0.412	0.273	0.010	0.012	0.177	0.350	0.226	0.444	0.227	0.334	0.492
HCG25F			0.006	0.042	0.941	-5.105		4.415	1.217	2.853	4.684
			0.011	0.013	0.205	0.405		0.503	0.255	0.375	0.564
HCG32A	-2.550	-0.238	0.079	0.118	1.054	-6.868	-2.026	5.670	1.676	3.268	6.692
	0.379	0.250	0.010	0.011	0.160	0.326	0.206	0.386	0.198	0.296	0.422
HCG32B	-2.252	0.179	0.062	0.111	1.349	-6.173		5.224	1.616	3.325	5.968
	0.478	0.313	0.011	0.013	0.204	0.412		0.497	0.253	0.371	0.546
HCG32D	-1.419	0.285	0.046	0.082	1.281	-6.123	-1.331	5.705	1.675	3.056	6.604
	0.466	0.311	0.011	0.013	0.205	0.393	0.257	0.498	0.248	0.367	0.543
HCG40A	-2.437	-0.109	0.097	0.136	1.095			5.373	1.606	3.253	7.312
	0.217	0.143	0.005	0.006	0.092			0.216	0.109	0.159	0.230
HCG40B	-1.911	0.269	0.060	0.094	1.295	-5.271	-1.209	4.965	1.728	3.321	6.992
	0.387	0.252	0.009	0.011	0.162	0.329	0.205	0.396	0.213	0.294	0.430
HCG42A	-2.090	-0.193	0.083	0.113	0.859	-6.301	-1.767	4.993	1.296	2.885	9.308
	0.290	0.192	0.008	0.009	0.143	0.300	0.185	0.378	0.204	0.313	0.480
HCG42C								4.265	1.256	3.021	6.072
								0.437	0.231	0.361	0.584
HCG62:ZM19	-2.415	-0.346	0.065	0.101	1.068	-5.938	-1.639	3.832	1.285	2.815	4.749
	0.509	0.340	0.012	0.014	0.217	0.429	0.270	0.532	0.266	0.388	0.570
HCG86A	-2.347		0.124	0.168	0.795	-6.981		5.021		2.892	7.032
	0.215		0.005	0.006	0.111	0.219		0.281		0.227	0.359
HCG86B			0.083	0.127	0.924	-6.588		5.210	1.205	2.879	6.345
			0.005	0.006	0.100	0.208		0.284	0.151	0.217	0.342

**Table A1.** Calibrated Lick indices. The data are *not* aperture corrected. Omitted indices are those lost to vignetting effects and those excluded from the estimation of derived parameters (Section 5).

comparison purposes. Interpretation of the data is discussed in the main body of the paper (Section 5).

### B1 Local abundance ratio correction

Estimates of [E/Fe] in the three studies are derived by comparison of Lick indices in galaxies to SSP estimates based on collections of local stars. These estimates are clearly mea-

surements of the difference between the [E/Fe] in the observed galaxies and that in local stars. This is important, as the abundance ratios of key elements (e.g. C, O and Mg) in stars in the solar neighbourhood have been shown to vary with [Fe/H], (Nissen & Edvardsson 1992; Edvardsson *et al.* 1993; Felzing & Gustafsson 1998; Gustafsson *et al.* 1999; Bensby *et al.* 2003). This effect must clearly be accounted for if we are to fully calibrate our estimates of [E/Fe] to the so-

Galaxy	H $\beta$	Fe5015	Mg $_1$	Mg $_2$	Mgb	Fe5270	Fe5335	Fe5406	Fe5709	Fe5782	[Mg/Fe]
<b>Loose Group</b>											
NGC 3305	1.490	5.723	0.172	0.346	5.198	2.665	2.445	1.641	0.989	0.788	3.644
	0.144	0.331	0.003	0.004	0.204	0.182	0.243	0.176	0.105	0.100	0.130
NGC 5046	1.539	5.406	0.155	0.320	4.779	2.843	2.533	1.855	0.876	0.839	3.584
	0.260	0.552	0.006	0.007	0.254	0.278	0.313	0.233	0.179	0.168	0.169
NGC 5049	1.443	5.274	0.140	0.302	4.507	2.873	2.524	1.655	0.829	0.812	3.487
	0.168	0.355	0.004	0.004	0.164	0.178	0.201	0.149	0.116	0.108	0.107
<b>Field</b>											
NGC 2502	1.230		0.155	0.319	4.991	2.861	2.511	1.661	0.865	0.837	3.661
	0.166		0.003	0.004	0.155	0.169	0.190	0.140	0.106	0.099	0.104
NGC 3203	2.029	6.158	0.130	0.284	4.144	3.061	2.791	1.850	0.995	0.990	3.482
	0.143	0.306	0.003	0.004	0.145	0.157	0.177	0.133	0.103	0.096	0.093
NGC 6684	2.104	6.081	0.122	0.273	3.957	2.924	2.716	1.890	1.083	1.029	3.340
	0.110	0.233	0.002	0.003	0.108	0.118	0.131	0.097	0.075	0.070	0.069
<b>Compact Group</b>											
HCG4C	2.279	6.266	0.117	0.262	4.162	3.125	2.415	1.715	1.022	0.978	3.395
	0.186	0.412	0.004	0.005	0.193	0.211	0.241	0.177	0.128	0.122	0.120
HCG16X	5.448	2.065	0.026	0.091	2.175	1.046	0.700	0.503	0.635	0.566	1.378
	0.201	0.493	0.005	0.006	0.227	0.261	0.300	0.223	0.170	0.163	0.173
HCG22A	1.431		0.170	0.333	4.935	2.955	2.475	1.795	0.992	0.895	3.660
	0.087		0.002	0.002	0.108	0.112	0.137	0.097	0.059	0.055	0.072
HCG22D	1.557	5.145	0.160	0.311	4.248	2.751	2.408	1.833	1.197	0.947	3.310
	0.187	0.399	0.004	0.004	0.189	0.197	0.229	0.168	0.117	0.112	0.122
HCG22E	1.480		0.111	0.265	4.082	2.680	2.059	1.736	1.365	0.769	3.110
	0.187		0.004	0.005	0.183	0.199	0.226	0.165	0.120	0.114	0.121
HCG22X	1.593	5.666	0.143	0.308	4.927	2.812	2.528	2.041	1.015	0.931	3.627
	0.202	0.460	0.004	0.005	0.235	0.240	0.294	0.224	0.151	0.146	0.155
HCG25F	2.235	4.904	0.073	0.216	3.292	2.911	2.342	1.651	0.943	0.541	2.940
	0.223	0.492	0.005	0.006	0.238	0.258	0.296	0.221	0.174	0.170	0.153
HCG32A	1.701	5.589	0.140	0.299	4.777	2.693	2.100	1.722	0.985	0.812	3.384
	0.168	0.370	0.004	0.004	0.176	0.186	0.216	0.201	0.118	0.112	0.159
HCG32B	1.813	5.211	0.121	0.270	4.666	2.695	2.248	1.757	1.120	0.754	3.396
	0.218	0.477	0.005	0.005	0.223	0.241	0.278	0.205	0.154	0.148	0.150
HCG32D	1.648	5.622	0.130	0.276	4.638	3.107	2.754	1.913	1.122	0.953	3.687
	0.215	0.463	0.004	0.005	0.216	0.233	0.266	0.197	0.146	0.139	0.140
HCG40A			0.146	0.306	4.594	2.390	2.492	1.909	0.915	0.819	3.349
			0.002	0.002	0.096	0.103	0.118	0.087	0.064	0.062	0.064
HCG40B	1.919	5.346	0.117	0.272	4.320	2.830	2.641	1.689	0.928	0.829	3.438
	0.172	0.381	0.004	0.004	0.180	0.201	0.235	0.171	0.125	0.120	0.121
HCG42A	1.337	5.321	0.160	0.314	4.523	2.827	2.367	1.570	0.852	0.814	3.427
	0.227	0.549	0.006	0.007	0.293	0.325	0.389	0.300	0.260	0.254	0.201
HCG42C	1.832	5.105	0.125	0.275	3.927	2.079	2.285	1.694	0.602	0.753	2.927
	0.263	0.624	0.007	0.008	0.328	0.377	0.435	0.333	0.303	0.294	0.229
HCG62:ZM19	1.616	4.224	0.119	0.280	4.563	2.487	1.766	1.629	0.818	0.423	3.115
	0.225	0.495	0.005	0.006	0.234	0.254	0.292	0.217	0.160	0.154	0.163
HCG86A		5.087	0.156	0.320	5.225	2.655	2.661	1.656	0.802		3.727
		0.426	0.004	0.005	0.270	0.253	0.346	0.256	0.188		0.178
HCG86B		4.799	0.118	0.269	4.364	2.645	2.363	1.505	0.591		3.306
		0.406	0.004	0.005	0.239	0.241	0.318	0.233	0.176		0.160

**Table A2.** Lick indices (as Table A1).

lar value. Indeed, it will be seen that, rather than being just a minor correction, consideration of this effect has a significant impact on correlations within the data. Consequently, this is a most important (and sometimes overlooked) aspect of the full calibration to the Lick system.

The most important elements for the analysis presented here are C, O, Mg, as these include the main elements upon which the enhancement sensitive indices used in this work (CN $_1$ , CN $_2$ , Ca4227, C $_2$ 4668, Mg $_1$ , Mg $_2$  and Mgb) are de-

pendent, and Fe to which the remainder of metallicity sensitive indices are most sensitive. We shall therefore concentrate on these elements in the discussion that follows.

Early studies of the pattern of abundance ratios in local stars (e.g. Nissen & Edvardsson 1992; Edvardsson *et al.* 1993) found that, in stars with [Fe/H]<0, strong anti-correlations exist between the abundances of various elements and [Fe/H]. The E group elements C, O and Mg were all shown to exhibit such a trend with a gradient  $\sim -0.5$

Galaxy	H $\delta_A$	H $\delta_F$	CN <sub>1</sub>	CN <sub>2</sub>	Ca4227	H $\gamma_A$	H $\gamma_F$	Fe4383	Ca4455	Fe4531	C <sub>2</sub> 4668
<b>Spiral Bulges</b>											
HCG4A			-0.038	-0.028	0.319			2.343	0.612	1.427	1.570
			0.006	0.007	0.107			0.268	0.134	0.208	0.314
HCG14A					0.964			3.772	1.058	2.719	5.076
					0.177			0.444	0.228	0.334	0.498
HCG14B		-0.323	0.056	0.082	1.113		-1.802	4.541	1.387	3.396	5.191
		0.240	0.009	0.010	0.153		0.193	0.369	0.184	0.252	0.403
HCG16A		1.980	-0.008	0.031	0.665	-1.870	0.742	3.997	1.271	2.298	5.411
		0.111	0.004	0.005	0.080	0.144	0.088	0.192	0.098	0.144	0.213
HCG16B	-2.807		0.088	0.115	1.046			5.519	1.558	3.313	6.742
	0.293		0.007	0.008	0.119			0.270	0.139	0.199	0.286
HCG22B	2.700	2.239	-0.083	-0.038	1.207	-1.383	1.471	3.052	1.032	2.849	4.179
	0.426	0.286	0.012	0.014	0.202	0.410	0.231	0.535	0.273	0.406	0.623
HCG25B			0.016	0.048	1.066	-4.825	-1.129	4.338	0.981	2.603	4.622
			0.012	0.014	0.209	0.399	0.252	0.489	0.246	0.351	0.504
HCG40D	1.574		-0.034	-0.015	0.577			3.382	0.905	2.007	4.017
	0.303		0.008	0.010	0.150			0.367	0.188	0.284	0.412
HCG62:ZM22	-1.335	0.412	-0.011	0.013	0.887			4.778	1.607	2.928	5.061
	0.547	0.359	0.013	0.016	0.235			0.553	0.246	0.407	0.595

Table A3. Lick indices (as Table A1).

Galaxy	H $\beta$	Fe5015	Mg <sub>1</sub>	Mg <sub>2</sub>	Mgb	Fe5270	Fe5335	Fe5406	Fe5709	Fe5782	[MgFe]
<b>Spiral Bulges</b>											
HCG4A			0.084	0.155	2.758	1.498	1.294	0.969	0.404	0.758	1.962
			0.003	0.003	0.122	0.139	0.157	0.116	0.090	0.085	0.092
HCG14B	1.507		0.122	0.271	4.185	2.370	2.090	1.386	0.774	1.059	3.055
	0.160		0.004	0.004	0.162	0.180	0.202	0.151	0.117	0.109	0.110
HCG14A			0.086	0.207	3.444	2.258	2.008	1.453	0.732	0.946	2.710
			0.004	0.005	0.202	0.221	0.250	0.184	0.142	0.133	0.132
HCG16A			0.097	0.217	3.374	2.430	2.151	1.406	0.899	0.941	2.780
			0.002	0.002	0.084	0.092	0.106	0.080	0.060	0.055	0.055
HCG16B			0.149	0.281		2.773	2.486	1.765	1.183	0.970	
			0.002	0.003		0.118	0.132	0.098	0.073	0.069	
HCG22B	3.105	4.612	0.060	0.174	2.708	2.179	1.759	1.175	0.983	0.743	2.309
	0.244	0.553	0.006	0.007	0.269	0.299	0.341	0.255	0.199	0.189	0.176
HCG25B			0.106	0.240	4.296	2.310	2.020	1.383	0.863	0.616	3.050
			0.004	0.005	0.175	0.194	0.217	0.159	0.115	0.109	0.124
HCG40D			0.077	0.185	3.419	1.915	1.632	1.054	0.641	0.619	2.462
			0.003	0.004	0.161	0.181	0.203	0.150	0.113	0.108	0.117
HCG62:ZM22	2.213	4.810	0.084	0.227	3.475	2.625	2.321	1.596	0.967	0.941	2.931
	0.229	0.497	0.005	0.006	0.234	0.254	0.287	0.213	0.165	0.156	0.150

Table A4. Lick indices (as Table A1).

dex/dex. However, these studies suggested that, at higher [Fe/H] these anti-correlations disappeared, with all stars with [Fe/H]>0 having solar abundance ratios. More recent work (incorporating non-LTE considerations) has changed this picture somewhat. The studies of Felzing & Gustafsson (1998), Gustafsson *et al.* (1999) and Bensby *et al.* (2003) showing that the trend seen at low metallicities continues at [Fe/H]>0, at least for O and C. It should be noted that C is the most important element in the estimation of indices in enhanced SSPs because, of the seven enhancement sensitive indices listed above, five are more sensitive to C than any other element. On the other hand, O is the element that dominates the E group in terms of mass. These two ele-

ments therefore dominate the mass of the E group elements as well as the sensitivities of the indices from which [E/Fe] is derived.

In the light of these findings the correction for the trend of decreasing [E/Fe] with [Fe/H], which was not included for [Fe/H]>0 in many preceding studies (including PS02), should be extended into this regime. To illustrate the effects of extending this correction Figures B1 and B2 show the results of terminating at [Fe/H]=0 and also continuing to higher [Fe/H]. We note that the lowest [Fe/H] in this study was -0.65 dex, well above the -1 dex at which the trends of elemental abundance with [Fe/H] change again (Felzing & Gustafsson (1998)). It can be seen in the plots of Figs B1

and B2 that this correction has profound effects on correlations in the data. For instance, weak  $[E/Fe]$ - $\log(\text{age})$  and  $[E/H]$ - $\log \sigma$  correlations are substantially strengthened by the correction, while an apparent correlation between  $[E/Fe]$  and  $\log \sigma$  is destroyed. A correlation also appears between  $[E/Fe]$  and  $[Fe/H]$  that was not apparent before application of the correction. This is not as surprising given that the magnitude of the correction is directly proportional to the  $[Fe/H]$  over the range it is applied. However, it is apparent that the correlation is only strengthened (not created) by the extension of the corrected regime to high  $[Fe/H]$ . It should also be noted that the extension to high  $[Fe/H]$  also has the effect of making the T00 and PS02 data consistent with those from the present study.



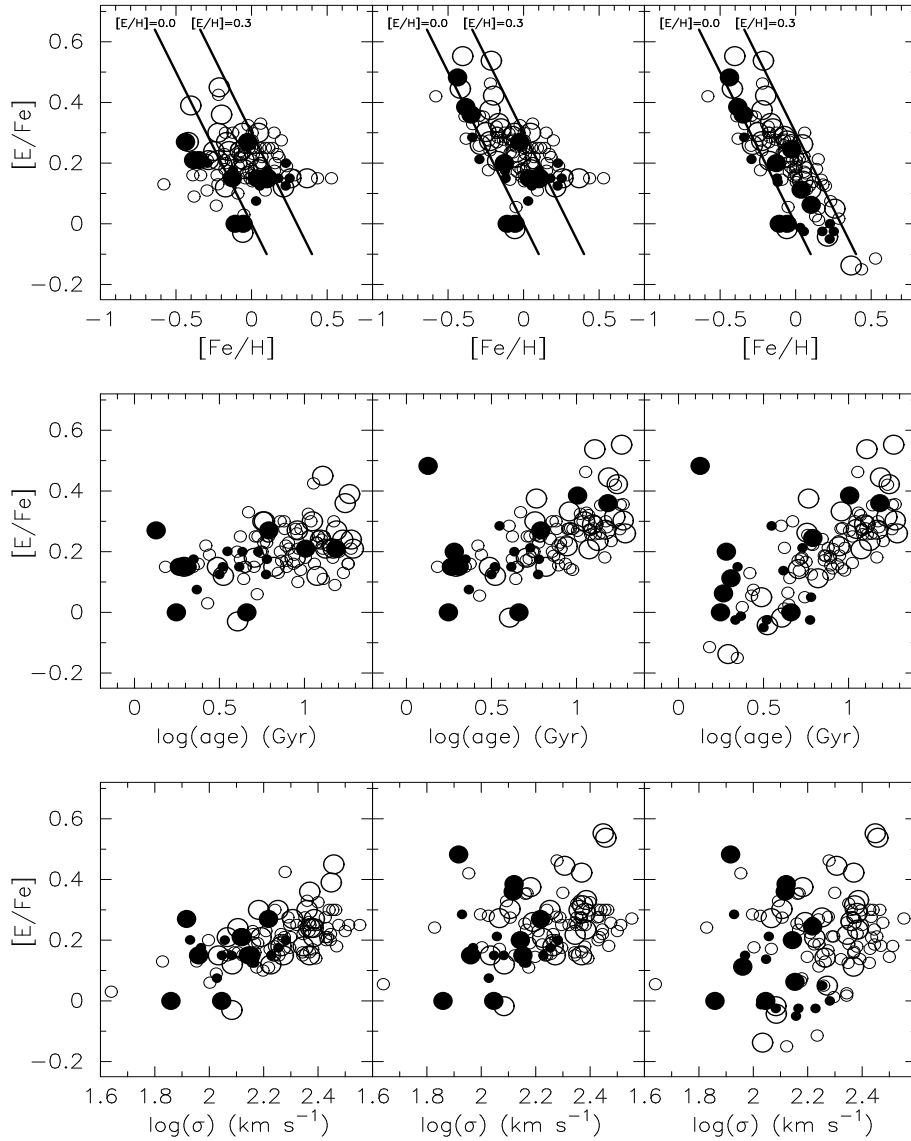


**Figure B1.** Derived parameters for the combined sample are plotted before and after correction for the local abundance ratio pattern. Spiral bulges are shown as filled circles. Large symbols are the present work while small symbols are the data from T00 and PS02. The left-hand panels show ‘raw’ data. Central panels show data after galaxies with  $[\text{Fe}/\text{H}] < 0$  have been corrected for the local abundance ratio trends. Right-hand panels show data when all galaxies have been corrected. Lines of constant  $[\text{E}/\text{Fe}]$  are shown in  $[\text{E}/\text{Fe}]$ – $[\text{Fe}/\text{H}]$  plots.

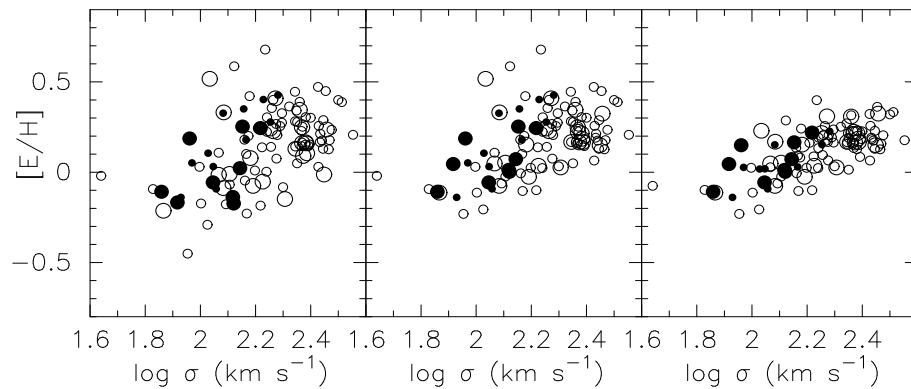


**Figure B2.** Symbols as Fig. B1. The correlations between  $[\text{E}/\text{H}]$  and  $\log \sigma$  are the same in early- and late-type galaxies

Galaxy	$\log(\text{age})_{\text{raw}}$	$\log(\text{age})_{\text{corr}}$	$[\text{Fe}/\text{H}]_{\text{raw}}$	$[\text{Fe}/\text{H}]_{\text{corr}}$	$[\text{E}/\text{Fe}]_{\text{raw}}$	$[\text{E}/\text{Fe}]_{\text{corr}}$
<b>EARLY TYPE</b>						
<b>Loose group</b>						
NGC 3305	1.225(0.075)	1.240(0.075)	-0.125(0.062)	-0.198(0.062)	0.360(0.050)	0.423(0.050)
NGC 5046	1.250(0.175)	1.275(0.175)	-0.125(0.113)	-0.249(0.113)	0.240(0.060)	0.303(0.060)
NGC 5049	1.150(0.100)	1.170(0.100)	-0.125(0.100)	-0.224(0.100)	0.210(0.030)	0.272(0.030)
<b>Field</b>						
NGC 2502	1.250(0.050)	1.287(0.050)	-0.100(0.062)	-0.286(0.062)	0.210(0.045)	0.260(0.045)
NGC 3203	0.500(0.125)	0.523(0.125)	0.325(0.125)	0.211(0.125)	0.120(0.030)	-0.042(0.030)
NGC 6684	0.250(0.112)	0.292(0.112)	0.575(0.150)	0.367(0.150)	0.150(0.045)	-0.137(0.045)
<b>Compact group</b>						
HCG4C	0.500(0.125)	0.488(0.125)	0.200(0.150)	0.259(0.150)	0.150(0.045)	0.050(0.045)
HCG16X	-0.126(0.075)	-0.111(0.075)	-0.200(0.100)	-0.273(0.100)	0.060(0.045)	0.160(0.045)
HCG22A	1.025(0.050)	1.047(0.050)	0.050(0.038)	-0.058(0.038)	0.300(0.015)	0.275(0.015)
HCG22D	1.225(0.100)	1.225(0.100)	-0.150(0.075)	-0.150(0.075)	0.240(0.060)	0.315(0.060)
HCG22E	1.075(0.150)	1.074(0.150)	-0.175(0.138)	-0.172(0.138)	0.120(0.060)	0.207(0.060)
HCG22X	1.125(0.100)	1.125(0.100)	-0.050(0.100)	-0.050(0.100)	0.210(0.060)	0.235(0.060)
HCG25F	0.600(0.188)	0.607(0.188)	-0.025(0.150)	-0.058(0.150)	0.030(0.060)	-0.017(0.060)
HCG32A	1.100(0.150)	1.095(0.150)	-0.100(0.113)	-0.074(0.113)	0.240(0.045)	0.290(0.045)
HCG32B	0.950(0.175)	0.945(0.175)	-0.075(0.150)	-0.050(0.150)	0.180(0.045)	0.218(0.045)
HCG32D	0.825(0.150)	0.820(0.150)	0.075(0.113)	0.099(0.113)	0.150(0.060)	0.113(0.060)
HCG40A	0.750(0.088)	0.756(0.088)	0.075(0.050)	0.046(0.050)	0.300(0.015)	0.263(0.015)
HCG40B	0.700(0.175)	0.706(0.175)	0.075(0.125)	0.047(0.125)	0.180(0.045)	0.143(0.045)
HCG42A	1.250(0.075)	1.266(0.075)	-0.325(0.062)	-0.403(0.062)	0.390(0.060)	0.553(0.060)
HCG42C	0.750(0.300)	0.764(0.300)	-0.150(0.175)	-0.222(0.175)	0.300(0.100)	0.375(0.100)
HCG62:ZM19	1.175(0.100)	1.189(0.100)	-0.350(0.088)	-0.419(0.088)	0.270(0.055)	0.445(0.055)
HCG86A	1.100(0.100)	1.108(0.100)	-0.175(0.087)	-0.213(0.087)	0.450(0.050)	0.537(0.050)
HCG86B	0.950(0.113)	0.958(0.113)	-0.125(0.100)	-0.165(0.100)	0.270(0.045)	0.333(0.045)
<b>SPIRAL BULGES</b>						
HCG4A	0.125(0.087)	0.127(0.087)	-0.425(0.138)	-0.437(0.138)	0.270(0.030)	0.483(0.030)
HCG14A	0.301(0.250)	0.309(0.250)	0.075(0.200)	0.037(0.200)	0.150(0.075)	0.113(0.075)
HCG14B	1.175(0.100)	1.184(0.100)	-0.300(0.075)	-0.347(0.075)	0.210(0.045)	0.360(0.045)
HCG16A	0.250(0.150)	0.264(0.150)	0.175(0.087)	0.103(0.087)	0.150(0.030)	0.063(0.030)
HCG16B	0.775(0.038)	0.790(0.038)	0.050(0.050)	-0.026(0.050)	0.270(0.015)	0.245(0.015)
HCG22B	0.225(0.051)	0.247(0.051)	0.000(0.113)	-0.108(0.113)	0.000(0.060)	0.000(0.060)
HCG25B	1.000(0.175)	1.007(0.175)	-0.350(0.137)	-0.383(0.137)	0.210(0.045)	0.385(0.045)
HCG40D	0.276(0.075)	0.281(0.075)	-0.100(0.125)	-0.127(0.125)	0.150(0.045)	0.200(0.045)
HCG62:ZM22	0.650(0.250)	0.661(0.250)	0.000(0.225)	-0.056(0.225)	0.000(0.060)	0.000(0.060)

**Table B1.** Results of age/metallicity determinations. Both raw data and data corrected for aperture effects and local abundance ratio patterns (Appendix B) are given.